SEISMIC ASSESSMENT OF SHAPE MEMORY ALLOY DAMPERS CONSIDERING SOIL-STRUCTURE INTERACTION BY RTHS

H. Ding[(1)], A. Kaup[(2)], J. Wang[(3)], L. Lu[(4)], O. Altay[(5)]

[(1)] *China Beijing, State Key Laboratory of Hydroscience and Engineering, Tsinghua University, dingh18@mails.tsinghua.edu.cn*
[(2)] *Germany Aachen, Department of Civil Engineering, RWTH Aachen University, kaup@lbb.rwth-aachen.de*
[(3)] *China Beijing, State Key Laboratory of Hydroscience and Engineering, Tsinghua University, wangjt@tsinghua.edu.cn*
[(4)] *China Beijing, State Key Laboratory of Hydroscience and Engineering, Tsinghua University, llq15@mails.tsinghua.edu.cn*
[(5)] *Germany Aachen, Department of Civil Engineering, RWTH Aachen University, altay@lbb.rwth-aachen.de*

Abstract

Superelastic shape memory alloys (SMAs) are metallic polycrystalline smart materials. SMAs can recover stress-induced strains up to 8 % almost without irreversible deformations and thus can control structural vibrations with their unique hysteric behavior. In fact, the energy dissipation arises from a hysteretic phase transformation from austenitic to martensitic grid structure and vice versa. As the hysteresis surface corresponds to the dissipated energy, dampers utilizing SMA wires must be designed in a way that the enclosed hysteresis area is maximized but the strain level of a total martensitic transition is not exceeded. More in detail, before phase transformation range, the material behavior resembles an elastic material response without hysteretic damping. For this purpose, the design procedure must include an accurate testing of the seismic response of the structure equipped with SMAs. However, conventional shaking table tests do not consider soil-structure interaction (SSI) effects, the occurrence of which is inevitable for structural buildings. This study proposes a real-time hybrid simulation (RTHS)-based seismic assessment framework of structures equipped with SMA wires, which considers the SSI effects. RTHS is a recently developed testing method, the idea of which is to split the entire system into a numerical substructure and a physical substructure. The numerical substructure of RTHS is utilized in this study to simulate the foundation-soil system with a finite-element model. Hence, in this study, two types of foundation conditions are taken into account: (a) a rigid foundation test, which is equivalent to a conventional shaking table test; and (b) a semi-infinite foundation test, which is a RTHS calculation with artificial viscoelastic boundary in a numerical substructure to simulate the radiation damping effects. Three recorded ground motions (El Centro, Kobe and Taft) are selected as seismic excitations. Furthermore, since the structural stiffness increases after the installation of SMA wires, stiffness-equivalent springs are installed to keep the structural stiffness approximately in line with the case of SMA wires as a set of control experiment. A comparison of the experimental results confirms that the hysteretic damping induced by SMA wires can effectively reduce the seismic response of structural buildings. However, the performance depends highly on the chosen design parameters and the strain-rate dependent seismic properties. According to the results, due to material and radiation damping of the soil foundation, the dynamic response of a structure changes significantly. Therefore, if the SSI effect is not considered during the design of the SMA parameters, the performance deviates or even deteriorates. Besides the RTHS results, the paper introduces the dynamic behavior of superelastic SMAs by the numerical simulation of some experiments. The results illustrate the dissimilar SMA damping behavior for experiments with SSI effects and rigid foundation experiments.

Keywords: shape memory alloy; real-time hybrid simulation; soil-structure interaction; structural control efficiency; macro-micro constitutive modeling

1. Introduction

Real time hybrid simulation (RTHS) testing is a recently emerging method for simulating the dynamic response of structures under seismic excitations [1]. Its main idea is to split the entire system into numerical substructure (calculated in the computer) and physical substructure (tested on the shaking table). The displacement and force coordination between the two substructures is considered in real-time to ensure the testing accuracy. Compared with the conventional shaking table tests, the RTHS makes it possible to perform large-scale or full-scale physical substructures tests considering the rate-dependent behavior of structures [2]. Numerous researchers have made efforts on improving the calculation scale, stability and numerical algorithms for the RTHS methods [3-5]. Meanwhile, several RTHS tests are conducted to investigate the structural dynamic response with different damper systems [6-8].

Nowadays, the number of high-rise engineering structures is surging due to the development of modern architectural design and construction. These structures exhibit high flexibility and low intrinsic damping. Furthermore, earthquakes cause a great challenge for civil engineering structures, as the seismic loading threatens both the safety and serviceability of structures. In order to increase the intrinsic damping and to mitigate seismic vibrations, several structural control strategies have been developed. Conventional anti-seismic devices, such as metallic steel dampers, are limited particularly regarding durability and maintenance. After each strong seismic event, most conventional devices which dissipate structural vibration energy by inelastic deformation need to be replaced because of non-recoverable plastic deformation.

As conventional inelastic damping device cannot recover deformations, researchers were motivated to research smart materials, such as superelastic shape memory alloys (SMAs). In fact, the unique hysteretic behavior of SMAs, allows to reduce structural vibrations without irreversible deformation. In this regard, researcher developed SMA wire based damping devices for bracing systems, buildings and bridges [9-11]. To numerically simulate the behavior of tensioned superelastic SMA wires under dynamic loads, researchers developed numerous one-dimensional, macroscopic material model [12, 13]. This study uses a developed more degree of freedom (MDoF) system with embedded macro-micro SMA constitutive model, to simulate bracing system controlled by SMA wires. The developed phenomenological macro-micro modelling approach is applied on a strain-rate dependent, thermomechanical coupled constitutive model [14]. The modeling approach can represent strain-rate dependent effects on the atomic lattice of SMA wires under dynamic loading and is based on a modeling approach to consider martensitic lattice destabilization of martensitic lattice in superelastic SMAs [15].

However, to evaluate the seismic response of a structure-damper system, the interaction between the structure and the soil foundation should be taken into account [16, 17]. When excited on a deformable soil foundation, the structure and the soil respond to the dynamics of each other simultaneously, which indicates that the dynamic characteristics as well as the seismic response characteristics are impossible to be independent of the soil-structure interaction (SSI) effects [18]. Investigations of SSI effects have revealed that the seismic response of the structure on soil foundations may show differences from those on rigid foundations [19]. Some relevant studies on soil–pile–structure interaction and SSI for wind turbines are conducted to reveal the real performance of structures under excitation [20, 21]. Therefore, it is of great significance to assess the control efficiency of SMA wires considering SSI effects, which present a more reliable assessment results and contribute to selecting reasonable parameters for the damper in the design stage. Nevertheless, SSI analyses through shaking table testing are problematic due to the fact that the semi-infinite soil foundation is difficult to implement in the laboratory. Generally speaking, laboratory-based SSI analyses employ specific designed soil containers, such as rigid container packed with foam at the sides, to simulate the semi-infinity of soil foundation [22]. However, the boundary effect of the finite soil container still influences the testing results. Moreover, the limited bearing capacity of the shaking table is an unavoidable problem when the experimenters try to place a large soil container and superstructures on the table. Alternatively, the RTHS testing method provides an effective way to deal with the above-mentioned difficulties due to its idea of substructures division [23, 24].

This study proposes a real-time hybrid simulation (RTHS)-based seismic assessment framework of structures equipped with SMA wires. On one hand, the numerical substructure of the RTHS is utilized in this study to simulate the foundation by setting the parameters of a finite-element soil model with artificial viscoelastic boundary to simulate the radiation damping effect [25]. On the other hand, a three-story steel frame is adopted as the physical substructure of the RTHS. Rigid foundation tests, which are equivalent to a conventional shaking table test, are also performed to investigate the case for the neglect of SSI effects. Three recorded ground motions (El Centro, Kobe and Taft) are selected as seismic excitations, respectively. For both types of foundation, experiments are conducted both on the uncontrolled structure and the controlled structure with SMA wires. As the structural stiffness increases after the installation of SMA wires, some stiffness-equivalent springs are furthermore used to keep the structural stiffness approximately in line with the case of SMA wires as a set of control experiment. Furthermore, the superelastic SMA behavior is simulated numerically, based on the experimental measured acceleration data, using a 3-DoF structural model with embedded constitutive SMA models between each floor. The experimental and numerical results provide helpful findings on parameters design optimization of the SMA damper to take maximum advantage of its damping properties.

2. Experimental RTHS system framework

In the Hydraulic Structure and Earthquake Engineering (HSEE) lab of Tsinghua University, a RTHS-based SMA wire testing system has been constructed, which couples a distributed real-time calculation subsystem, a MTS shaking table subsystem, a real-time data acquisition-transmission subsystem and a three-story steel frame used as the controlled structure, see Fig.1. The distributed real-time calculation system, built by using xPC target toolbox in MATLAB, is employed to solve the equations of motion in real-time and to generate displacement signals [24]. The loading system consists of an oil source and a shaking table with a 1.5 m × 1.5 m working area, a bearing capability of 2 tons, and a maximum acceleration of 1.2 g. The data acquisition-transmission system uses PXI and LabVIEW real-time module to construct the data acquisition platform. Shared common random-access memory network (SCRAMNet) cards are utilized to guarantee data transfer between two substructures in real-time [23].

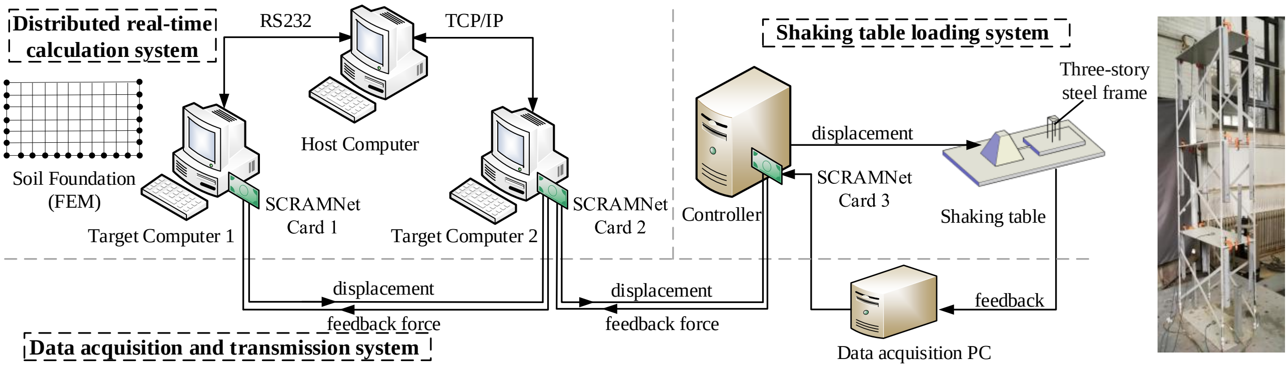

Fig. 1 – Outline of the RTHS-based SMA wire testing system

2.1 Physical substructure

In this RTHS-based work, the physical substructure consists of a three-story steel frame and SMA wires or equivalent-stiffness steel springs. The steel frame is applied as the controlled structure; its size is designed to adopted to the shaking table size. Specifically, each floor is 0.61 m in length, 0.3 m in width, and 1 cm in thickness. The supporting leg is 1 cm in the side length, and 0.69 m in length. X-shaped braces are mounted perpendicular to the excitation direction to ensure the lateral and torsional stiffness of the frame model. In addition, to enable the installation of SMA wires and steel springs at the frame, in total 18 steel L-profiles are installed at the frame model. The L-profiles serve to connect the floors to apply the interstory drift on the damping systems. Finally, the mass of each floor is 14.37 kg, while the total mass of the whole steel frame reaches 72.06 kg with additional device. The SMA wires with a 0.2 mm diameter and a 10 mm length are mounted between two L-profiles. Analogously, springs with a spring-rate of 2.29 N·mm^{-1} are used to keep the stiffness approximately in line with the case of SMA wires as a set of control experiment. Four accelerometers are installed on the frame to measure the acceleration and calculate the displacement of each floor. One is placed directly on the shaking table to record the exact shaking table movement and the others respectively on the positive center of each floor. Besides, some strain gauges attached on the legs of the frame are implemented to measure the strain through the Wheatstone bridge method. The shear force measuring between the two substructures is able to be realized by stastic force calibration which aims to bulid a relationship between the strain and force. The above-mentioned SMA wires, springs and measuring apparatuses are illustrated in Fig.2.

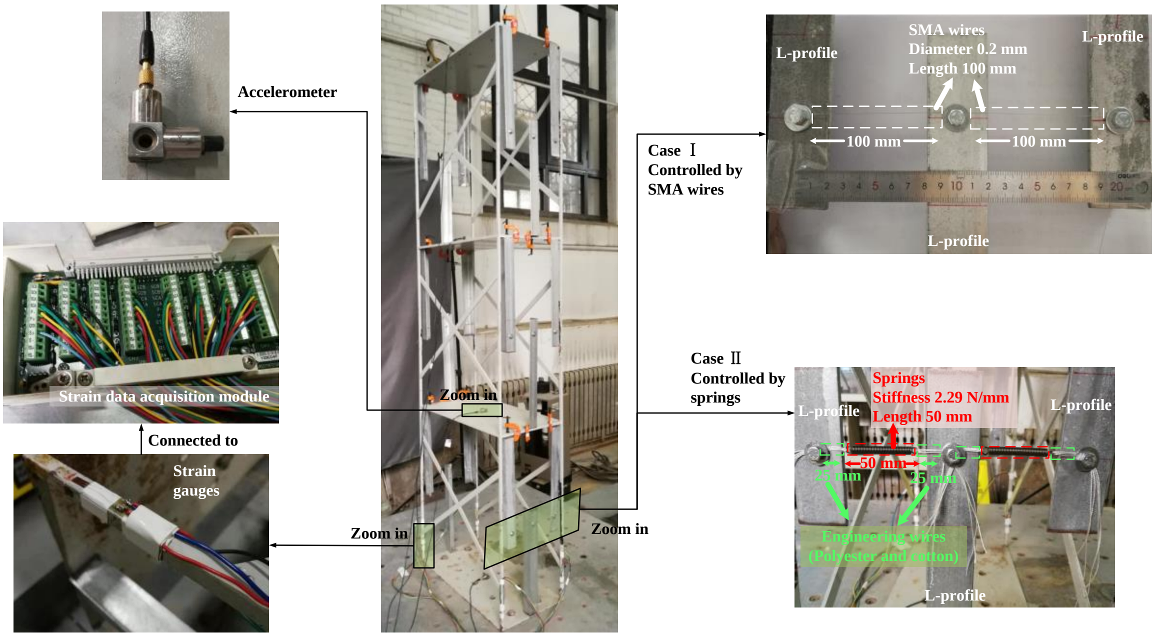

Fig. 2 – Close-up views of the installed SMA wires, springs and measuring apparatuses

2.2 Numerical substructure

The numerical substructure of the RTHS framework is a finite-element soil model with artificial viscoelastic boundary [25]. It is constructed by a user-compiled finite-element analysis block, which is combined in MATLAB-Simulink S-function to call syntax and to execute a real-time RTHS calculation. More in detail, springs and dashpots are applied on the boundary nodes of the model to simulate the radiation damping effect in the semi-infinite foundation. As shown in Fig.3, the FEM foundation model is 20 m × 10 m with the 2 m × 2 m mesh size, thus it is discretized into 66 nodes and 50 square solid elements with 132 degrees of freedom. The parameters of the prototype soil are setting as follows: the mass density is 2000 kg/m^3, the elastic modulus is 200 MPa, and the Poisson's ratio is 0.2.

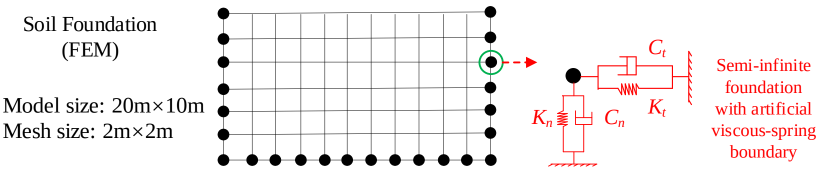

Fig. 3 – Finite-element soil model with artificial viscoelastic boundary

2.3 Experimental scale

In dynamic tests, it is necessary to consider the similarities of material and dynamic properties. The similitude ratio and soil foundation parameters are determined in this subsection to achieve the soil foundation parameters that matches the three-story frame model parameters. For convenience and security, we construct the small-scale three-story frame model described in Section 2.1 as physical substructure. Assuming that the frame model has the same natural frequencies and damping ratio as the prototype, the basic experimental scales are set as: the natural frequency scale $C_f = 1$, the damping ratio scale $C_\zeta = 1$, the acceleration scale $C_a = 1$, the displacement scale $C_u = 1$, the mass scale $C_m = 400$, the damping scale $C_c = 400$, the stiffness scale $C_k = 400$. Subsequently, the prototype superstructure has a mass of 28824 kg. Based on the prototype soil parameters stated in Section 2.2 and the experimental scales, the properties of the soil model can be obtained: an elastic module of 0.5 MPa, a density of 5 kg·m^{-3}, a Poisson's ratio of 0.2.

2.4 Numerical algorithm and delay compensation

To analyze the numerical substructure in real-time, the Gui-λ numerical algorithm method with unconditionally stable condition (λ = 4) is used [4]. Besides, a polynomial based forward prediction algorithm for real-time dynamic sub-structuring is introduced into the numerical calculation part to ensure that the RTHS system does not occur instability due to the inevitable time delay [26].

2.5 Numerical MDoF frame structure with constitutive SMA wire model

A two-dimensional 3-DoF lumped mass model with embedded strain-rate dependent constitutive model for superelastic SMAs is implemented in the MATLAB-Simulink environment to recalculate the experimental results. The lumped mass model has its DoF only in the vibration direction. Therefore, the floors are assumed to be rigid and a column deformation is neglected.

To simulate the 3-story steel frame structure with SMA, the equation of motion (EoM) reads,

$$\mathbf{M}\ddot{x} + \mathbf{C}\dot{x} + \mathbf{K}x + f_S(x) = f(t) \tag{1}$$

with $\ddot{x}$, $\dot{x}$ and x representing the acceleration, velocity and displacement vectors for each DoF of the structure. The entries for the mass matrix **M** are resulted from the structure dimension to m_1=m_2=25.45 kg and m_3=21.09 kg. Further, the stiffness matrix **K** is calculated for each floor with the equivalent member method to $k_{1,2,3}$=16.22 kN·m^{-1}. Next, the damping matrix **C** is formulated according to the Rayleigh damping,

$$\mathbf{C} = \alpha\mathbf{M} + \beta\mathbf{K} \tag{2}$$

where the Rayleigh damping coefficients α and β are calculated as follows

$$\begin{bmatrix} \alpha \\ \beta \end{bmatrix} = \frac{2\omega_1\omega_2}{\omega_2^{\;2} - \omega_1^{\;2}} \begin{bmatrix} \omega_2 & -\omega_1 \\ -\dfrac{1}{\omega_2} & \dfrac{1}{\omega_1} \end{bmatrix} \tag{3}$$

The damping ratios D_1=0.0245 and D_2=0.0203 originate from free oscillation tests according to the first and second natural mode of the structure. With the natural frequencies, listed in Table 1, the Rayleigh damping coefficients α and β can be calculated to receive finally C_1=C_3=0.0222 and C_2=0.0122 for the damping matrix. Last, $f_S(x)$ represents the nonlinear restoring forces induced by the SMAs depending on the displacements of the structure as

$$f_S(x) = \left(f_{S,1}, \cdots, f_{S,n}\right)^{\mathrm{T}} \quad \text{with} \;\; f_{S,i} = \sum\nolimits_j \sigma_j A_j \tag{4}$$

where the force resulting from each SMA wire j, which is acting on the DOF i. The stress σ_j is the tensile wire stress calculated in the constitutive model and A_j is the corresponding wire cross-sectional area. To solve the EoM, the numerical algorithm from Section 2.4 is used.

3. Vibration control assessment tests considering SSI effects by RTHS

The results of RTHS-based shaking table tests of the uncontrolled and the controlled structure are discussed in this section. For the controlled structure, it is mounted with superelastic SMA wires in one case and steel springs in the other case. For the uncontrolled structure, there is no connection between the L-profiles. In total, the experimental procedure comprises white noise tests and seismic ground motions tests for both, the rigid foundation and semi-infinite foundation. Three recorded ground motions (El Centro, Kobe and Taft) are selected as seismic excitations whose dominant frequencies are approximately 0.5 ~ 10 Hz. The ground motions cover near-field (Kobe, Taft) and far-field (El Centro) earthquakes.

3.1 White noise tests

The experimental system identification works are carried out through the white noise tests to obtain the natural frequency. The identification tests are performed for three different physical substructures, i.e., (a) an uncontrolled steel frame, (b) a frame controlled by SMA wires, (c) a frame controlled by springs; and for two different soil foundations, i.e., (a) rigid foundation, (b) semi-infinite foundation. The first two natural frequencies of the RTHS experimental system are calculated accordingly by fast Fourier transformation (FFT), as summarized in Table 1. It can be observed that, for these two cases, i.e., (a) with SMA wires and (b) with the stiffness-equivalent springs, the natural frequencies of the system will increase to a similar level, compared with the uncontrolled case. In addition, for the case of semi-infinite foundation, the natural frequencies may be slightly lower than the rigid case. This is caused by the dynamic characteristic of the system changes when the SSI effects are introduced. In fact, the SSI leads to longer natural periods of vibration and higher damping ratios.

Table 1 – Natural frequencies of the tested system configurations

Soil foundation	Physical substructure	1st natural frequency/ Hz	2nd natural frequency/ Hz
Rigid	Uncontrolled	1.89	6.12
	With SMA wires	2.26	8.01
	With springs	2.18	7.11
Semi-infinite	Uncontrolled	1.84	6.06
	With SMA wires	2.22	7.89
	With springs	2.14	7.03

3.2 Seismic tests

The experimental seismic tests comprise three historical records of earthquake motion, i.e., El Centro with scaled peak ground acceleration (PGA) of 0.07 g, Kobe and Taft with scaled PGA of 0.05 g. The selected PGA levels are chosen to aim that SMA wires deformation strain does not exceed the 8 % strain limit, which retains their re-centering and damping capability. In fact, the PGA levels occur from preliminary conventional shaking table tests on the structure controlled by SMA wires and are chosen to have a maximum relative story drift of 6 % strain. Fig.4 and Fig.5 plot the displacement time histories of the physical substructure under seismic loading for rigid and semi-infinite foundation, respectively. From Fig.4, it is clear that the responses decrease to some extent with springs, whereas much more significantly with SMA wires. Hence, Fig.4 demonstrates that the SMA wires have a significant damping effect for earthquake induced vibrations on the rigid foundation experimental setup. Actually, the comparable good damping behavior of the steel springs occurs from several effects, i.e., the friction between engineering wires and L-profiles, damping effects of the engineering wires which connect the springs with the L-profile and the additional stiffness on the system. Nevertheless, the installed SMA wires, with their superelastic damping effects, perform best for all three earthquakes when SSI is not taken into account. However, when SSI effects are considered, the displacement responses decrease significantly for all three different physical substructures, which is easily found by comparing Fig.4 and Fig.5. This results from the dissipated vibration energy of the radiation waves when SSI is considered. In fact, the SSI system has a higher damping ratio, because the damping effect of soil is introduced into the system. Comparing Fig.4(a1) and Fig.5(a1) it is apparent that, in this test campaign, even the uncontrolled system is significantly damped due to the SSI damping effects. In fact, the superelastic damping of the SMA wires decreases as the system is already previously damped by the SSI damping effects.

The displacement differences between the uncontrolled structure and the controlled structure with SMA wires in Fig.4(a1) and Fig.5(a1) decreases for the semi-infinite foundation compared to the rigid foundation. To further illustrate the here observed SSI effect, Fig.6 shows the interlayer drifts of the physical substructure (SMA wires case only) for rigid and semi-infinite foundation. After considering the SSI effect, the strain of SMA wires decreases predominantly, which influences the damping properties of SMA wires. However, it should be noted that the SSI effect in some parts even intensifies the strain and thus the observed effects must not be generalized. The damping properties of the SSI strongly depend on the soil-model, soil-parameters, excitation signal and the tested physical structure.

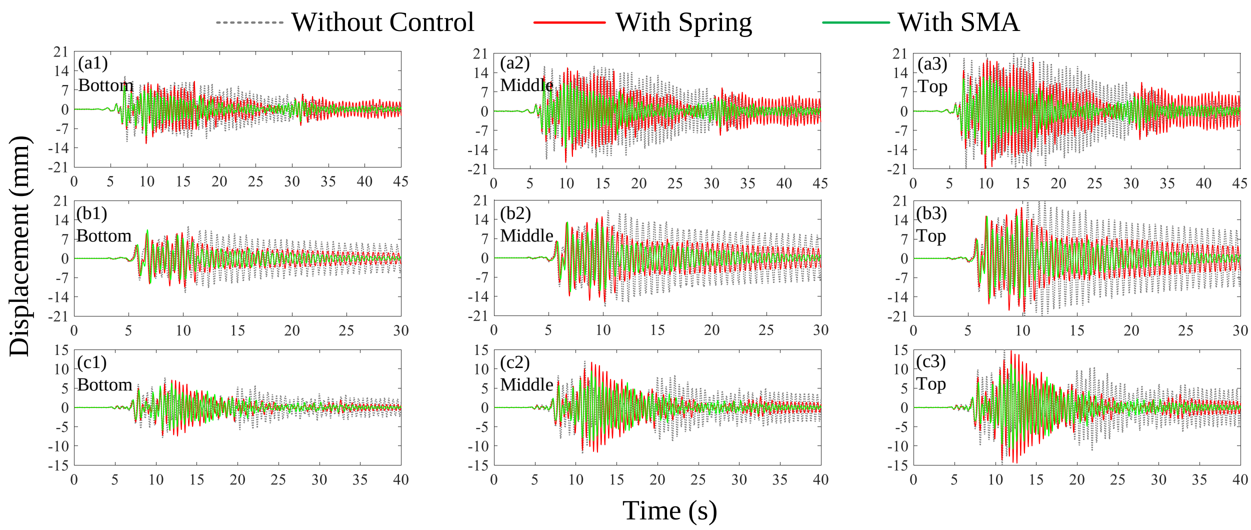

Fig. 4 – Displacement time histories of dynamic responses for rigid foundation under seismic load. (a) El Centro, (b) Kobe and (c) Taft

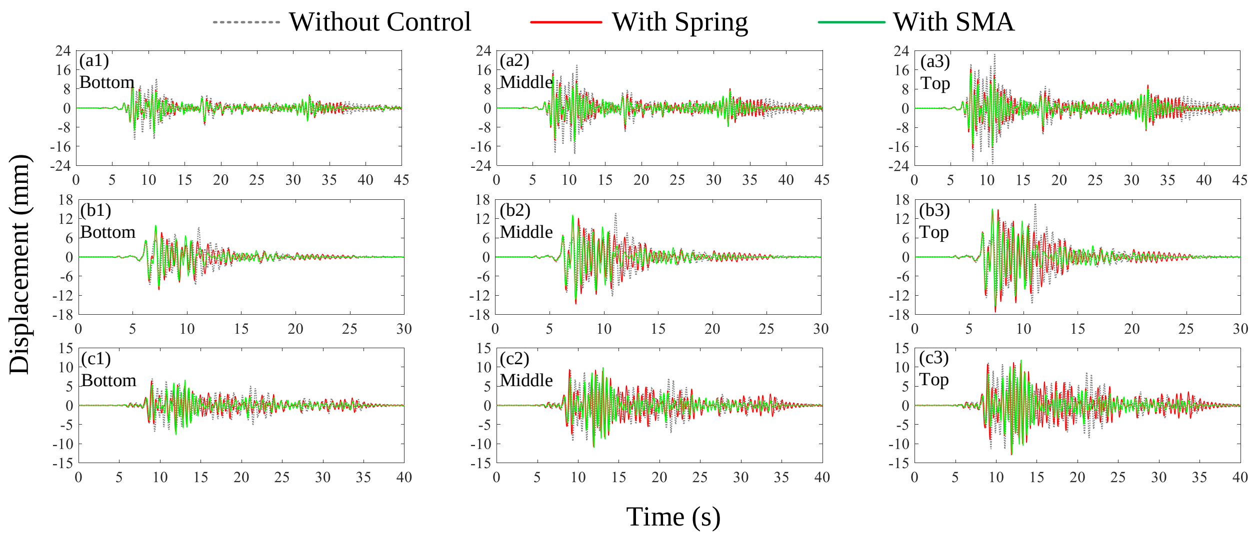

Fig. 5 – Displacement time histories of dynamic responses for semi-infinite foundation under seismic load. (a) El Centro, (b) Kobe and (c) Taft

To compare the displacement responses of the uncontrolled and controlled structure with (a) SMA wires and (b) steel springs more in detail, we define a factor denoted as R_d to represent the proportion of RMS displacement decline, as expressed in Eq. (5). Fig.7 shows the R_d values of RMS displacement response for rigid and semi-infinite foundation. Compared to the uncontrolled physical substructure, the case with springs provides additional stiffness, while the controlled structure by SMA wires provides damping from the superelastic property of SMA wires and almost the same stiffness as springs. Thus, the difference between the R_d values of SMA wires and those of the springs on the same foundation approximately reflects the superelastic damping effect of SMAs on the RMS displacement response.

$$R_d = 1 - \frac{RMS\left(x_{controlled}\right)}{RMS\left(x_{uncontrolled}\right)} \tag{5}$$

Based on the above analysis, we can roughly estimate the damping effect of the SMA wires from the difference between the solid line and the dotted line in the same color in Fig.7. The difference between the R_d values of SMA wires and steel springs for the semi-infinite foundation compared to the rigid foundation decreases significantly. Indeed, the differences of $R_{d,SMA}$ to $R_{d,Spring}$ values of the bottom, middle and top layer are 28.2 %, 32.8 %, 34.7 % for El Centro; 14.9 %, 19.8 %, 20.5 % for Kobe; and 14.6 %, 22.2 %, 23.5 % for Taft under the rigid foundation. Whereas, under the semi-infinite foundation, the differences are 4.3 %, 9.4 %, 12.1 % for El Centro; 9.0 %, 13.5 %, 15.8 % for Kobe; and 4.3 %, 14.2 %, 15.9 % for Taft. This reveals that the control efficiencies of the SMA wires considering the SSI effect are lower compared to the rigid foundation. In other words, it proves that structures and foundation should be taken into account as a whole for an optimized SMA wire damper design.

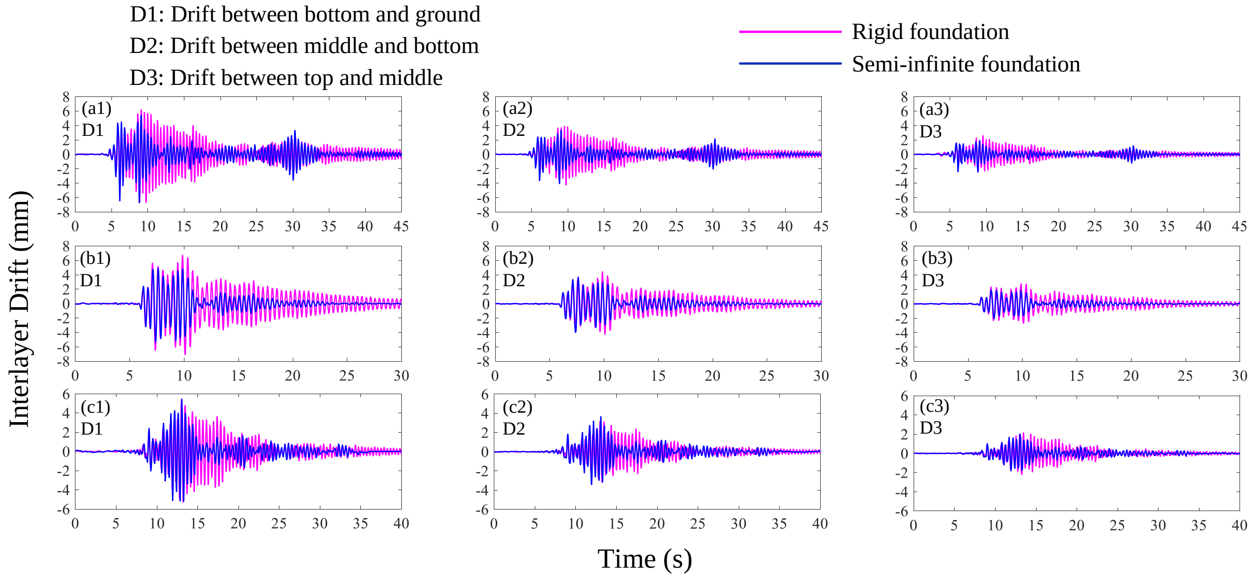

Fig. 6 – Interlayer drift of physical substructure (SMA wires case) for rigid and semi-infinite foundation under seismic load. (a) El Centro, (b) Kobe and (c) Taft

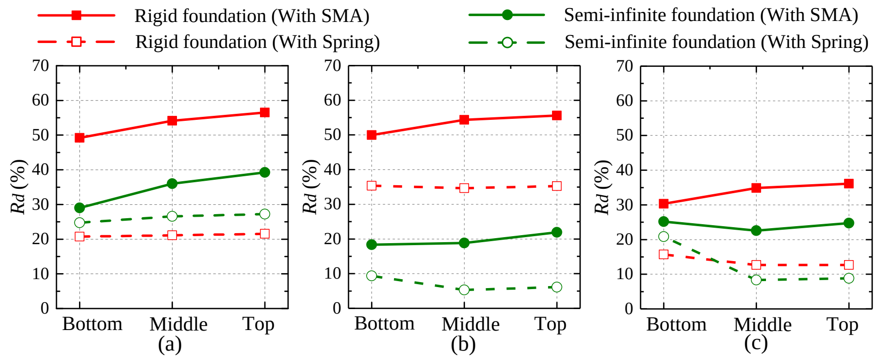

Fig. 7 – Proportion of RMS displacement decline for rigid and semi-infinite foundation under seismic load. (a) El Centro, (b) Kobe and (c) Taft

The decreasing SMA damping efficiency in the absence of design optimization is also proven with the numerical recalculation of the El Centro earthquake experiment. In addition, the embedding of the constitutive SMA model in the 3-DoF model enables to directly determine the superelastic hysteresis and the resulting dissipated energy. Fig.8 illustrates the stress-strain curves for the attached SMA wires between the ground and the bottom floor. The load history is comparable to the interlayer drift in Fig.6(a1). However, the results originate from the numerical 3DoF frame structure with embedded constitutive SMA wire model. The input signal for the calculation is the respective experimental measured acceleration data from the accelerometer, which is placed directly on the ground of the shaking table, see Fig.9(a) for semi-infinite foundation. Indeed, Fig.8 exemplifies the superelastic damping is activated significantly more for the rigid foundation (a) compared to semi-infinite foundation (b). This can be also proven by the calculated dissipated energy E_D. The dissipated energy corresponds to the hysteresis surface calculation from the force-displacement curves and is measured in N·mm. The calculation results a dissipated energy E_D of 1298.97 N·mm for the rigid foundation experiment and 573.10 N·mm for the SSI experiment. Hence, with absence of SMA design optimization, the dissipated energy of the SMA wires decreases significantly.

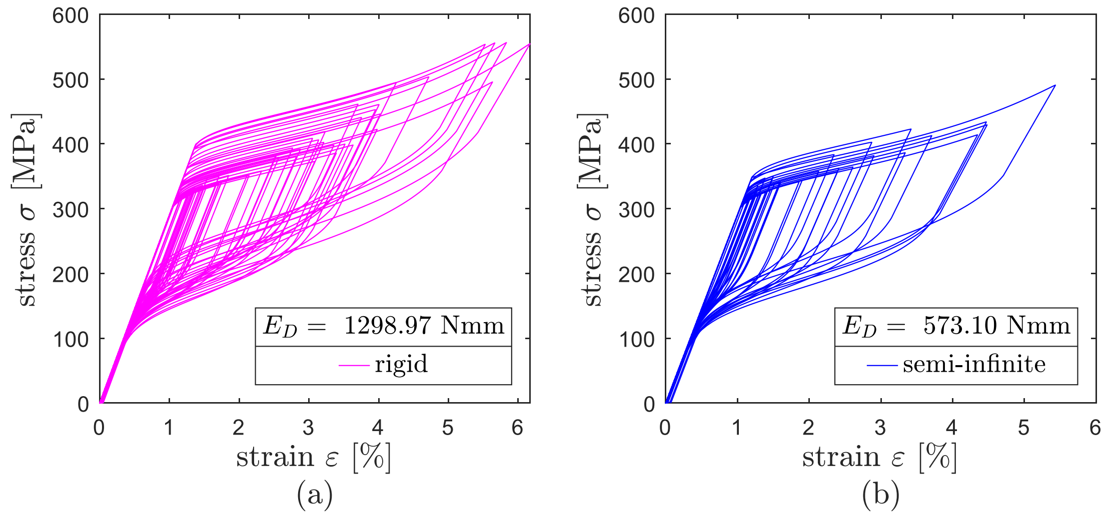

Fig. 8 – Numerical simulation with the 3-DoF frame structure with embedded constitutive SMA wire model. Calculation of the stress-strain curves of SMA wires installed between bottom and ground for the El Centro earthquake with (a) rigid foundation and (b) semi-infinite foundation. Calculation of the dissipated energy E_D corresponding to the hysteresis surface.

To proof the accuracy of the numerical model, Fig.9 illustrates exemplarily, for the El Centro earthquake with semi-infinite foundation, a comparison of the numerical and experimental results for the acceleration of the bottom floor, Fig.9(b), and the displacement, Fig.9(c), respectively. Further, we introduce the factors ΔR_x and $\Delta R_{\ddot{x}}$ as,

$$\Delta R_x = \frac{RMS\left(x_{experimental}\right)}{RMS\left(x_{numerical}\right)} \tag{6}$$

and

$$\Delta R_{\ddot{x}} = \frac{RMS\left(\ddot{x}_{experimental}\right)}{RMS\left(\ddot{x}_{numerical}\right)} \tag{7}$$

to compare the RMS values of the numerical and experimental displacement and acceleration data. The numerical acceleration RMS value agrees 97.8 % with the experimental RMS value. Also, the comparison of the displacement RMS value provides quite accurate results, as the accordance is 92.4 %. Therefore, the comparisons in Fig.9 prove that the previously calculated stress-strain curves are reliable and thus allow a statement about the SMA wire performance. Concluded, the SMA wires are loaded for the more realistic RTHS-SSI calculation in a different strain range. As a result, less energy is dissipated if the design is not adapted to the SSI effects. Accordingly, the RTHS-SSI calculation should be considered to optimize the SMA wire design.

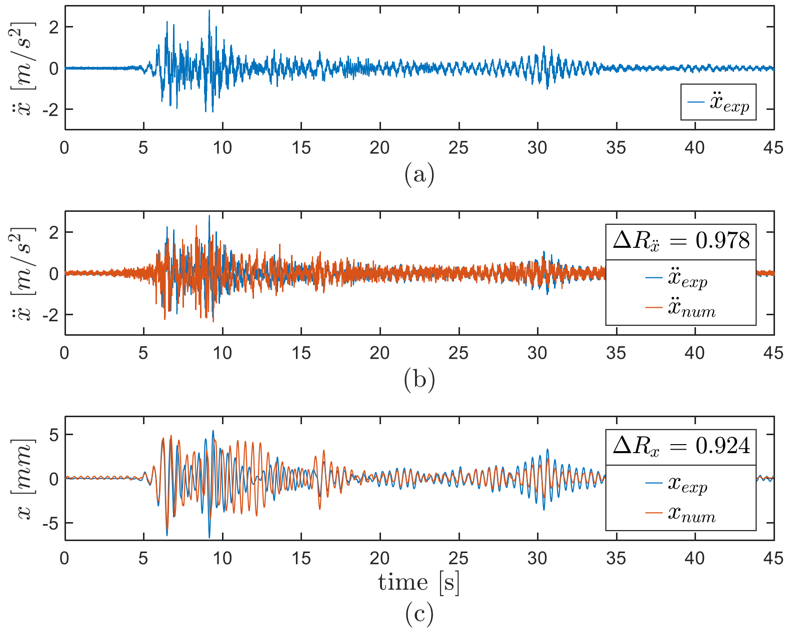

Fig. 9 – Numerical results (orange line) compared to experimental results (blue line) for the El Centro earthquake with semi-infinite foundation. (a) ground acceleration from experimental results as input for the numerical calculation. (b) acceleration of the bottom floor; comparison of the acceleration RMS values $\Delta R_{\ddot{x}}$. (c) displacement of the bottom floor; comparison of the displacement RMS values ΔR_x.

4. Conclusion

This paper presented a RTHS-based seismic assessment framework of structures equipped with SMA wires. For illustration, a three-story steel frame test structure with SMA wires was investigated by shaking table tests. The wires were originally designed for the structure without considering SSI effects. In RTHS, a numerical FE model was used to include SSI effects in the investigation and assess the damping performance of SMAs more accurately. Historic near- and far-field ground motions (El Centro, Kobe, and Taft) were used. The tests included the uncontrolled structure, the two controlled cases with SMA wires and with stiffness-equivalent steel springs. The results were compared with the rigid foundation without soil model. In both cases, SMAs could reduce the vibrations of the structure. However, in RTHSs with SSI effects the SMA performance deviated or even deteriorated. Besides RTHSs, numerical simulations were performed to investigate the SMA wire performance more accurately. The stress-strain curves of the SMA wires were calculated by numerically simulating the RTHS investigations using a numerical model of the frame structure with constitutive SMA models. The results confirmed that the damping estimation of SMAs may deviate when the SSI effect is ignored. Accordingly, the design of SMA based damping devices must include the SSI effect.

5. Acknowledgements

The authors would like to express their sincere appreciation for the financial support from the National Natural Science Foundation of China (NSFC) with the grant number 51725901 and the German Research Foundation (Deutsche Forschungsgemeinschaft, DFG) with the grant number 322268262.

6. Copyrights

7. References

[1] Nakashima M, Kato H, Takaoka E (1992): Development of real-time pseudo dynamic testing. *Earthquake Engineering & Structural Dynamics*, **21** (1), 79-92.

[2] Zhu F, Wang JT, Jin F, Zhou MX, Gui Y (2014): Simulation of large-scale numerical substructure in real-time dynamic hybrid testing. *Earthquake Engineering & Engineering Vibration*, **13** (4), 599-609.

[3] Ahmadizadeh M, Mosqueda G, Reinhorn AM (2008): Compensation of actuator delay and dynamics for real-time hybrid structural simulation. *Earthquake Engineering & Structural Dynamics*, **37** (1), 21-42.

[4] Gui Y, Wang JT, Jin F, Chen C, Zhou MX (2014): Development of a family of explicit algorithms for structural dynamics with unconditional stability. *Nonlinear Dynamics*, **77** (4), 1157-1170.

[5] Bonnet PA, Lim CN, Williams MS, Blakeborough A, Neild SA, Stoten DP, Taylor CA (2007): Real-time hybrid experiments with newmark integration, MCSmd outer-loop control and multi-tasking strategies. *Earthquake Engineering & Structural Dynamics*, **36** (1), 119-141.

[6] Zhu F, Wang JT, Jin F, Lu LQ (2017): Real-time hybrid simulation of full-scale tuned liquid column dampers to control multi-order modal responses of structures. *Engineering Structures*, **138**, 74-90.

[7] Nguyen TT, Dao TN, Aaleti S, Van De Lindt JW, Fridley KJ (2018): Seismic assessment of a three-story wood building with an integrated CLT-lightframe system using RTHS. *Engineering Structures*, **167**, 695-704.

[8] Zhang RY, Phillips BM, Fernández-Cabán PL, Masters FJ (2019): Cyber-physical structural optimization using real-time hybrid simulation. *Engineering Structures*, **195**, 113-124.

[9] Dolce M, Cardone D, Marnetto R (2000), Implementation and testing of passive control devices based on shape memory alloys. *Earthquake Engineering & Structural Dynamics*, **29** (7), 945-968.

[10] Auricchio F, Fugazza D, Desroches R (2006). Earthquake performance of steel frames with nitinol braces. *Journal of Earthquake Engineering*, **10**, 45-66.

[11] Ozbulut OE, Roschke P (2010). GA-based Optimum Design of a Shape Memory Alloy Device for Seismic Response Mitigation, *Smart Materials and Structures*, **19**, 065004.

[12] Aurrichio F and Sacco E (2001). Thermo-mechanical modeling of a superelastic shape-memory wire under cyclic stretching-bending loadings. *International Journal of Solids and Structures*, **38**, 6123-45.

[13] Ren W, Li H, Song G (2007). A one-dimensional strain-rate-dependent constitutive model for superelastic shape memory alloys. *Smart Materials and Structures*, **16** 191-7.

[14] Zhu S and Zhang Y (2007). A thermomechanical constitutive model for superelastic SMA wire with strain-rate dependence. *Smart Materials and Structures*, **16** 1696-707.

[15] Kaup A, Altay O, Klinkel S (2020). Macroscopic modeling of strain-rate dependent energy dissipation of superelastic SMA dampers considering destabilization of martensitic lattice. *Smart Materials and Structures*, **29** (2), 025005.

[16] Kausel E (2010): Early history of soil–structure interaction. *Soil Dynamics & Earthquake Engineering*, **30** (9), 822-832.

[17] Lou ML, Wang HF, Chen X, Zhai YM (2011): Structure–soil–structure interaction: Literature review. *Soil Dynamics & Earthquake Engineering*, **31** (12), 1724-1731.

[18] Pitilakis D, Dietz M, Wood DM, Clouteau D, Modaressi A (2008): Numerical simulation of dynamic soil–structure interaction in shaking table testing. *Soil Dynamics & Earthquake Engineering*, **28** (6), 453-467.

[19] Iguchi M (1978): Dynamic interaction of soil–structure with elastic rectangular foundation. *Proceeding of the fifth Japanese Earthquake Engineering Symposium*, Tokyo, Japan.

[20] Hokmabadi AS, Fatahi B, Samali B (2014): Assessment of soil–pile–structure interaction influencing seismic response of mid-rise buildings sitting on floating pile foundations. *Computers & Geotechnics*, **55**, 172-186.

[21] Fitzgerald B, Basu B (2016): Structural control of wind turbines with soil structure interaction included. *Engineering Structures*, **111**, 131-151.

[22] Mizuno H, Sugimoto M, Mori T, Iiba M, Hirade T (2000): Dynamic behavior of pile foundation in liquefaction process-shaking table test utilizing big shear box. *Proceeding of the 12th World Conference on Earthquake Engineering*, Auckland, New Zealand.

[23] Wang Q, Wang JT, Jin F, Chi FD, Zhang CH (2011): Real-time dynamic hybrid testing for soil–structure interaction analysis. *Soil Dynamics & Earthquake Engineering*, **31** (12), 1690-1702.

[24] Zhou MX, Wang JT, Jin F, Gui Y, Zhu F (2014): Real-Time Dynamic Hybrid Testing Coupling Finite Element and Shaking Table. *Journal of Earthquake Engineering*, **18** (4), 637-653.

[25] Liu JB, Li B (2005): A unified viscous-spring artificial boundary for 3-D static and dynamic applications. *Science in China Series E-Engineering & Materials Science*, **48** (5), 570-584.

[26] Wallace MI, Wagg DJ, Neild SA (2005): An adaptive polynomial based forward prediction algorithm for multi-actuator real-time dynamic substructuring. *Proceedings: Mathematical, Physical and Engineering Sciences*, **461** (2064), 3807-3826.

